Journal of Cluster Science (2018) 29:1305–1311
https://doi.org/10.1007/s10876-018-1450-y

ORIGINAL PAPER

The Density Functional Theory Investigation on the Structural, Relative Stable and Electronic Properties of Bimetallic Pb_nSb_n (n = 2–12) Clusters

Gaofeng Li[2,3] · Xiumin Chen[1,2,3] · Hongwei Yang[2,3] · Baoqiang Xu[2,3] · Bin Yang[2,3] · Dachun Liu[2,3]

Received: 6 March 2018 / Published online: 12 September 2018

Abstract

Recently, bimetallic clusters have attracted a great deal of attention from research community because clusters yield intriguing properties ranging from the molecular and the bulk materials, which have extensive applications in nanomaterials. Clusters with tailored properties are governed by cluster size, geometrical structures, and elemental composition. Motivated by that we systematically investigated the structural, relative stable, and electronic properties of Pb_nSb_n (n = 2–12) clusters by means of density functional theory. In this paper, the ground state structures, average binding energies, fragmentation energies, HOMO–LUMO gaps, and density of states were theoretically calculated. The results demonstrate that the large clusters adopt distorted ellipsoid structures with no symmetry. The average binding energies tend to be stable when cluster size $n \geq 4$. Pb_5Sb_5 and Pb_9Sb_9 clusters are more chemically stable compared with the neighboring Pb_nSb_n clusters, which may serve as the cluster assembled materials. The density of states of Pb_nSb_n (n = 2–12) clusters moving toward more negative energy levels with the growing cluster size n, which also becoming more nonlocalized as the clusters size n increasing.

Keywords Bimetallic clusters · Geometrical structures · Density functional theory · Electronic properties · Pb_nSb_n clusters

Introduction

The main investigations of cluster science are to investigate the essential properties of clusters and promising applications of clusters in nanomaterials, which making an essential bridge between the molecules and macro materials [1–3]. During the past several decades, the pure clusters composed of group IV or group V elements have been highly investigated by scholars from all over the world. As an example, the growth behaviors and fundamental properties of C_n clusters [4–6], Si_n clusters [7, 8], Ge_n clusters [9, 10], Sn_n clusters [11, 12], Pb_n clusters [13, 14], As_n clusters [15, 16], and Sb_n clusters [17, 18] have been systematically investigated by both experiments and DFT calculations. Although many investigations have proved that the pure clusters or binary clusters from the same group of the periodic table elements have many similar properties [19–22] since the similar electronic configurations of the elements and analogous geometric structures of clusters. However, the investigations of bimetallic clusters are of great interest and significance due

Electronic supplementary material The online version of this article (https://doi.org/10.1007/s10876-018-1450-y) contains supplementary material, which is available to authorized users.

✉ Xiumin Chen
chenxiumin9@hotmail.com

[1] State Key Laboratory of Complex Nonferrous Metal Resources Clear Utilization, Kunming University of Science and Technology, Kunming 650093, People's Republic of China

[2] National Engineering Laboratory for Vacuum Metallurgy, Kunming University of Science and Technology, Kunming 650093, People's Republic of China

[3] Yunnan Provincial Key Laboratory for Nonferrous Vacuum Metallurgy, Kunming University of Science and Technology, Kunming 650093, People's Republic of China

to the valence electron configurations of the both elements are different, thus bimetallic clusters may yield intriguing properties which show huge differences to both of the pure clusters.

Pb is the group IV element while Sb is the group V element. Therefore, they are the particularly evident p-block elements. The semiconductor materials consist of group III–V elements have contributed to the modern electronics, since scientist had discovered C_{60} which have exploited a new material field in carbon nanotubes and fullerenes. The discovery of cluster assembled materials with tunable properties by fine-tuning of element composition and geometrical structures are significant. It is well known that clusters are different from their molecules and condensed matters. Moreover, the physical and chemical properties of clusters are different with their size n, geometrical structures, and chemical composition. Therefore, it is crucial to elucidate the relationship between the clusters' properties and their cluster size n for a given chemical composition system.

So far, Pb_n clusters, Pb-based clusters, Sb_n clusters, and Sb-based clusters have been systematically investigated. For Pb_n clusters, the clusters with small cluster size n adopt planar structures while large clusters possess three dimensional structures. In addition, Pb_n clusters demonstrate a metal-to-nonmetal transition with growing cluster size n. The cluster formation and ionization of Pb_n clusters were analyzed by Saito et al. [23] using the time-of-flight mass spectrometer. Rajesh et al. [24] investigated the geometrical structures and electronic structures of Pb_n and Pb_n^+ (n = 2–15) cluster using density functional theory. Sascha et al. [25] carried out a molecular beam experiment to study the electric deflection of Pb_n (n = 7–38) clusters. Senz et al. [26] applied the core–hole photoelectron spectroscopy as a probe to study lead clusters, it was found that lead clusters demonstrate a metal-to-nonmetal transition which is in well accordance with density functional theory calculations. For Sb_n clusters, in the vapor phases, Sb tends to form tetrahedral clusters which are similar to the P_4 cluster, As_4 cluster. Polak et al. [1] investigated Sb^-, Sb^{2-}, Sb^{3-}, and Sb^{4-} clusters by photoelectron spectra. Zhou et al. [20] theoretically calculated the structural and electronic properties of Sb_n (n = 2–10) clusters within density functional theory. Bernhardt et al. [19] investigated the decomposition mechanisms of Sb_n^+ (n = 3–12) clusters versus cluster size n, surface type, as well as collision energy using surface collision induced dissociation mass spectrometry. In terms of bimetallic Pb-based and bimetallic Sb-based clusters, Rajesh et al. [27] theoretically investigated Pb_nM (M = C, Al, In, Mg, Sr, Ba, and Pb; n = 8, 10, 12, and 14) clusters, in order to investigate the effects of impurity M atoms on structural and electronic properties Pb_n clusters through comparing the differences between Pb_n clusters and Pb_nM clusters. Chen et al. [28] investigated the structural and magnetic properties of MPb_{10} and $[MPb_{10}]_2$ (M = Fe, Co, and Ni) clusters using density functional theory. Steinert et al. [29] synthesized the Mn/Sb clusters in the silicon matrix in order to explore the formation of MnSb clusters.

There are some experimental investigations on the growth pattern and content intensity properties of PbSb clusters [21, 22, 30–33]. According to the experimental results involving mass-spectrometer-based methods [32, 33], the PbSb, Pb_2Sb_2, Pb_3Sb_3, and Pb_4Sb_4 clusters were observed, demonstrating that the bimetallic Pb_nSb_m clusters with equal molar ratio of Pb atoms and Sb atoms were found with enhanced stability. Furthermore, the binding energies of clusters were detected by photoelectron spectroscopy [21]. However, the Pb_nSb_n ($n > 4$) clusters were not achieved by experiments. It is believed that the larger clusters are difficult to be generated compared with the smaller clusters, even the larger cluster are difficult to be detected by experimental devices owing to the limited resolution of instruments [34].

Density functional theory has been proved to be an efficient and powerful tool to investigate the physical and chemical properties of clusters, because the calculated results can be in well agreement with the experimental ones [34, 35]. Although some bimetallic clusters composed of Pb and Sb have been investigated using experiments and DFT calculations, there are scarce data for the Pb_nSb_n clusters larger than Pb_4Sb_4 cluster. In this paper, the structural and electronic properties of Pb_nSb_n (n = 2–12) have been investigated by means of density functional theory. We firmly believe that the fundamental investigation of Pb_nSb_n clusters is interesting and vital, which may exceed to find cluster-assembled nanomaterials and novel properties.

Computational Methods

In the present work, all calculations were performed using DFT method, as implemented in the $DMol^3$ code [20, 36, 37]. The ground state structures of Pb_nSb_n clusters were achieved by the following steps. Firstly, the starting structures of Pb_nSb_n clusters were built based on the ground state structures of $Pb_{n-1}Sb_{n-1}$ clusters. The structures of Pb_nSb_n clusters were extensively searched by ab initio molecular dynamics, where time step is 1 fs, total simulation time is 100 ps. Secondly, following geometrical optimizations were performed based on the local minimal energy structures of ab initio molecular dynamics. Thirdly, the energy calculations were carried out based on the optimized structures. Finally, the ground state structures of Pb_nSb_n clusters can be obtained through comparing the

energies of the different structures of Pb_nSb_n clusters. The singlet spin was used for the Pb_nSb_n clusters with even numbers of electrons, whereas the double spin was used for the Pb_nSb_n clusters with odd numbers of electrons during geometrical optimizations. Because the higher spin state, the higher energy of the structure was obtained. The spin unrestricted and formal spin as initial was used during energy calculations and ab initio molecular dynamics. The PBE functional within the general gradient approximation (GGA) was employed to treat exchange and correlation interactions [20, 28, 38, 39]. The DFT-semi-core potential was used to replace the internal electrons of Pb_nSb_n systems. The basis set is double numerical basis combined with polarized functions (DNP). The SCF calculations were performed till the change of total energy is less than 10^{-6} Ha. The convergence standards of force and energy: the maximum force is less than 10^{-5} Ha $Å^{-1}$, the energy per atom is converged to 10^{-5} Ha $Å^{-1}$, and the maximum displacement is converged to 0.005 Å. The charge and spin involving density mixing standard are 0.2 and 0.5, respectively. The smearing (0.005 Ha) was used in order to achieve good convergence results. In addition, the direct inversion in iterative subspace (DIIS) method was also used in order to speed up the calculations and reduce calculation costs [40, 41]. The frequency calculations were performed to ensure that the lowest energy structures of Pb_nSb_n (n = 2–12) clusters are located on the true minima of the corresponding potential surfaces. The parameters of Sb_2 and Pb_2 dimers were calculated in order to confirm the reliability of GGA–PBE functional for Pb_nSb_n systems. In this work, the calculated bond length, vibrational frequency, total binding energy, and vertical ionization potential of Sb_2 dimer are 2.574 Å, 260.52 cm^{-1}, 2.82 eV, and 8.18 eV, respectively, while the corresponding experimental data are 2.49 Å [42], 270 cm^{-1} [43], and 3.1 eV [19], and 9.275 eV [43]. The calculated bond length, vibrational frequency, and vertical ionization potential of Pb_2 dimer are 2.961 Å, 119.65 cm^{-1}, 6.46 eV, respectively, and the experimental data are 2.93 Å [36], 110 cm^{-1} [36], 6.2 eV [23], respectively. It is obvious that the calculated parameters excellently agree with the experimental ones. Therefore, the calculation methods in this work are reliable.

Results and Discussion

Ground State Structures and Vibrational Spectra of Pb_nSb_n (n = 2–12) Clusters

Here, the lowest energy structures of Pb_nSb_n (n = 2–12) clusters were focused, because all the properties of Pb_nSb_n clusters were calculated based on the lowest energy structures. All the structures are the energetic minima structures because the lowest energy structures were verified with no imaginary frequency. The lowest energy structures of Pb_nSb_n (n = 2–12) clusters are displayed in Fig. 1, and the atomic coordinates of lowest energy structures of Pb_nSb_n (n = 2–12) clusters are shown in Tables S1–S11 (the details can be seen in the supporting information). As it is shown in Fig. 1, the Pb_2Sb_2 cluster favors a triangular pyramid structure, and its point group symmetry is C_2. It has been shown that Pb_4 cluster adopts a planar structure [44], whereas Sb_4 cluster also forms a triangular pyramid structure [20] which is similar to the geometrical structure of Pb_2Sb_2 cluster. Pb_3Sb_3 cluster forms a structure which a Pb atom and a Sb atom bind together and capped on the same side of the parallelogram. In addition, Pb_3Sb_3 cluster exhibits C_s symmetry. For Pb_4Sb_4 cluster, a distorted bilayer parallelogram with no symmetry is the most stable structure of Pb_4Sb_4 cluster. Pb_5Sb_5 cluster is composed of two parts, one part is a distorted pentagonal pyramid, and the other part is a distorted quadrangle. The point group symmetry of Pb_5Sb_5 cluster belongs to C_s. The ground state structure of Pb_6Sb_6 cluster is similar to that of Pb_5Sb_5 cluster, shows point group symmetry of C_2. Pb_7Sb_7 cluster with C_s symmetry is a cage-like structure, and most of the surfaces show distorted quadrangle structures and rest of the surfaces show triangle structures. Pb_8Sb_8 cluster possesses C_1 point group symmetry. The ground state structure of Pb_8Sb_8 cluster likes a distorted ellipsoid structure. It is interesting to point out that Pb_nSb_n (n = 9–12) clusters also adopt ellipsoid structures, which show no symmetry. According to the Jahn–Teller distortion theorem, the lower symmetry can lower the energies of the clusters [45–47]. Therefore, it may be the reason why the large clusters with no symmetry are energetically favorable. On the basis of the growth pattern of Pb_nSb_n (n = 2–12) clusters, the large clusters tend to adopt distorted ellipsoid structures and prefer no symmetry.

Here, the vibrational spectra of Pb_nSb_n (n = 2–12) clusters were calculated in order to provide the comparison for experimental results, because the cluster structures can be determined by comparing the calculated spectra and experimental spectra, and the calculated results would provide additional theoretical information for the experimental results. The vibrational spectra of Pb_nSb_n (n = 2–12) clusters are shown in Fig. S1 (the details can be seen in the supporting information). The vibrational frequencies of Pb_nSb_n clusters are in the range of 0–250 cm^{-1}. The location of vibrational frequencies, the relative intensities of vibrational peaks, as well as the shapes of vibrational peaks are the important signals to identify the structures of Pb_nSb_n clusters.

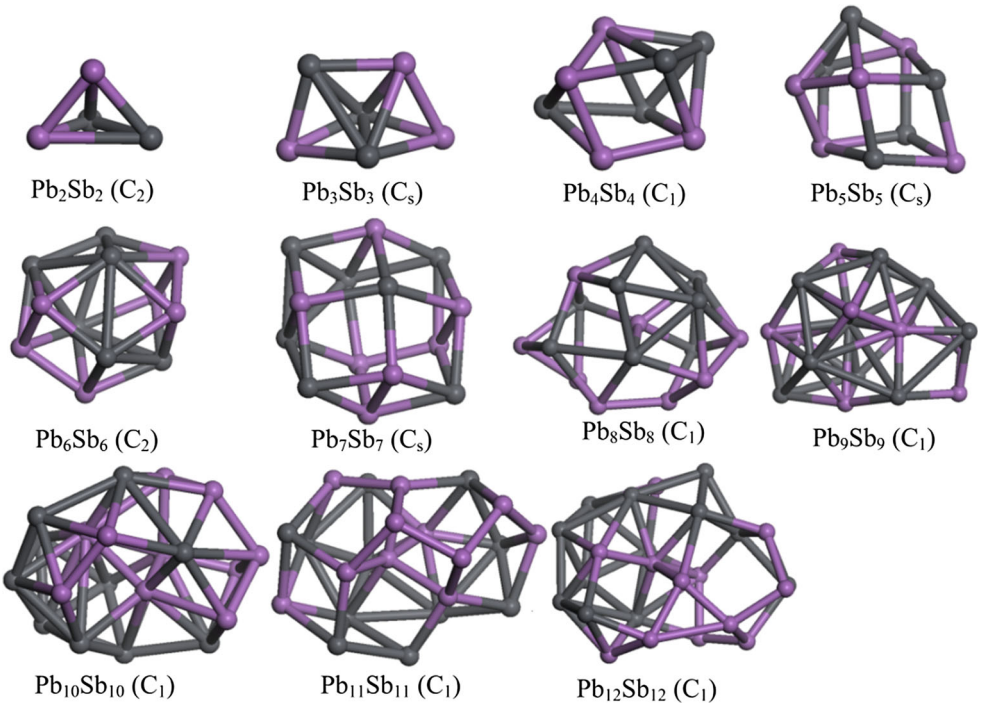

Fig. 1 The lowest energy structures of Pb_nSb_n (n = 2–12) clusters. The corresponding point group symmetry is shown in the parentheses. The purple ball is Sb atom, and the gray ball is Pb atom

Relative Stable and Electronic Properties of Pb_nSb_n (n = 2–12) Clusters

The stable properties of Pb_nSb_n (n = 2–12) clusters were calculated on the basis of the lowest energy structures. The binding energy per atom (E_b) of Pb_nSb_n cluster can be calculated using the formula [48–51]

$$E_b = [nE(Pb) + nE(Sb) - E(Pb_nSb_n)]/2n$$

where E(Pb), E(Sb), $E(Pb_nSb_n)$ are the energies of Pb atom, Sb atom, and Pb_nSb_n cluster, respectively. Hence, the average binding energy is a good index to describe the thermodynamic properties of Pb_nSb_n cluster. Figure 2 shows the average binding energies of Pb_nSb_n clusters as a function of cluster size n. Firstly, average binding energies increase sharply with the increasing size n when cluster size n are in the range of n = 2–4, then average binding energies approach stable when size $n \geq 4$. Therefore, the geometrical structures of Pb_nSb_n (n = 2–12) clusters tend to be stable when cluster size $n \geq 4$.

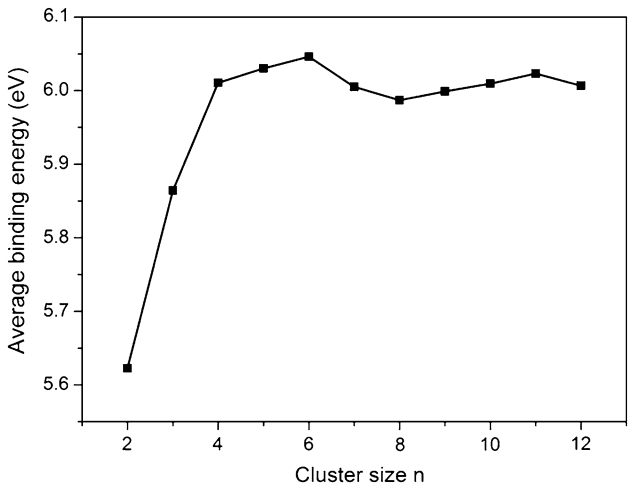

Fig. 2 The average binding energies of Pb_nSb_n (n = 2–12) clusters as a function of cluster size n

The fragmentation energy (ΔE) can demonstrates the relative stabilities of Pb_nSb_n clusters compared with their neighboring clusters. The definition of ΔE can be defined as [52]

$$\Delta E(Pb_nSb_n) = E(Pb_{n-1}Sb_{n-1}) + E(PbSb) - E(Pb_nSb_n)$$

where $E(Pb_{n-1}Sb_{n-1})$, E(PbSb), and $E(Pb_nSb_n)$ represent the total energies of the $Pb_{n-1}Sb_{n-1}$ cluster, PbSb cluster, and Pb_nSb_n cluster, respectively. ΔE as a function of cluster size n for Pb_nSb_n clusters is shown in Fig. 3. The fragmentation energies show that there are some obvious oscillating behaviors. Several local peaks are found at n = 4, 6, 9, and 11, revealing that Pb_4Sb_4 cluster, Pb_6Sb_6 cluster, Pb_9Sb_9 cluster and $Pb_{11}Sb_{11}$ cluster are more thermodynamically stable compared with the neighboring Pb_nSb_n clusters. In general, the fragmentation energies show a decrease trend as the cluster size n increasing.

In order to analyze the chemical stabilities of Pb_nSb_n clusters, the HOMO–LUMO gaps of Pb_nSb_n (n = 2–12) clusters were calculated. The HOMO–LUMO gap is a significant parameter to reflect the chemical stability of a cluster, which demonstrates the energy gap between the

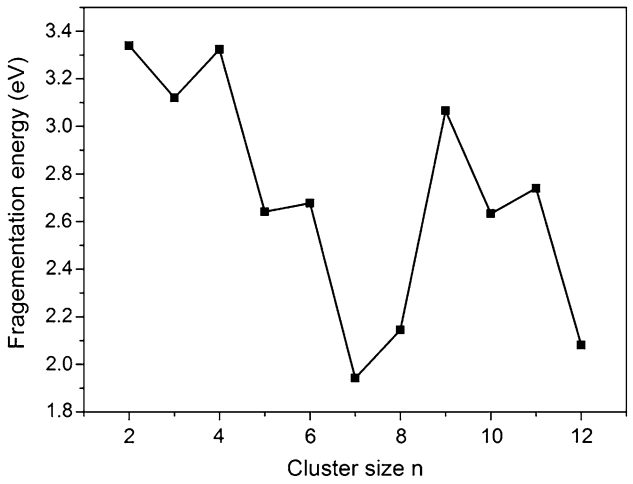

Fig. 3 The fragmentation energies of Pb_nSb_n (n = 2–12) clusters as a function of cluster size n

highest occupied orbital and the lowest unoccupied orbital [53]. A higher value of HOMO–LUMO gap represents that the cluster is more chemically stable, whereas a smaller value of HOMO–LUMO gap exhibits that the cluster is more chemically unstable. The HOMO–LUMO gaps of Pb_nSb_n (n = 2–12) clusters as a function of cluster size n is shown in Fig. 4. From the Figure, we can see that there are obvious oscillations within the cluster size range of n = 2–12. In general, the trend of HOMO–LUMO gaps decrease with the increasing cluster size n. The two local maxima of HOMO–LUMO gaps are found at n = 5 and n = 9. The local maxima of HOMO–LUMO gaps of Pb_nSb_n clusters suggest that Pb_5Sb_5 cluster and Pb_9Sb_9 cluster are chemically stable compared with the neighboring

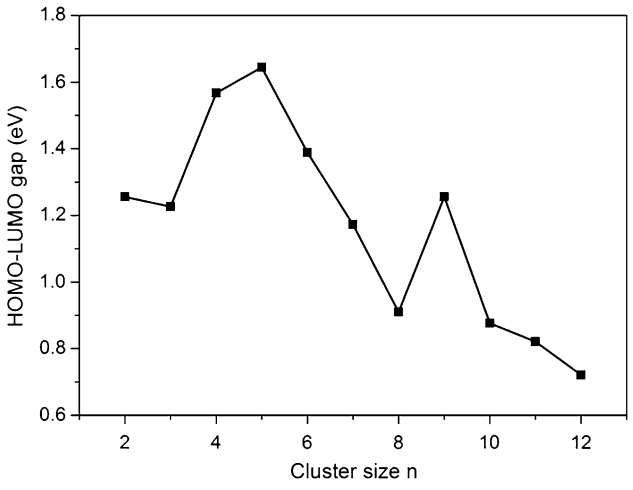

Fig. 4 The HOMO–LUMO gaps of of Pb_nSb_n (n = 2–12) clusters as a function of cluster size n

Pb_nSb_n clusters. Furthermore, Pb_5Sb_5 cluster and Pb_9Sb_9 cluster have great potential in cluster assembled materials due to their chemical stabilities.

In order to well understand the electronic properties of Pb_nSb_n (n = 2–12) clusters, the density of states of Pb_nSb_n (n = 2–12) clusters were calculated, as shown in Fig. 5. In the present work, the density of states near fermi levels were focused because those density of states near the fermi levels are significant. From the Figures, the obvious trend of density of states of Pb_nSb_n clusters can be observed, which density of states move toward more negative energy levels with increasing cluster size n. In other words, the fermi levels shift to more positive energy levels with increasing cluster size n. The most positive energy levels of conduction bands tend to be stable and approach stable at 0.08 Ha. For the density of states near the fermi levels, the contributions of p electrons are the maximum, the contributions of s electrons are the minimum, and that of d electrons are in between p electrons and s electrons. Hence, the p electrons have the largest contributions to the fermi levels, which may be originated from that the Pb and Sb elements are the evident p-block elements. For the density of states in the range of $-0.5 \sim -0.2$ Ha, the s and p electrons almost have the same contributions, whereas d electrons have the smallest contributions. For the density of states in the range of 0.01–0.4 Ha, the p and d electrons have the equal contributions while s electrons have smallest contributions. Moreover, density of states becoming more nonlocalized with the growing clusters size n, demonstrating that the metallicity of Pb_nSb_n clusters becoming more predominant with the growing clusters size n.

Conclusions

In the present work, the structural, relative stable and electronic properties of Pb_nSb_n (n = 2–12) clusters have been systematically investigated in the frame work of density functional theory. The Pb_nSb_n clusters with large size n prefer distorted ellipsoid structures and demonstrate no symmetry. The average binding energies of Pb_nSb_n clusters tend to be stable when cluster size $n \geq 4$. On the basis of fragmentation energies, Pb_4Sb_4 cluster, Pb_6Sb_6 cluster, Pb_9Sb_9 cluster and $Pb_{11}Sb_{11}$ cluster are more thermodynamically stable compared with their neighboring Pb_nSb_n clusters. Pb_5Sb_5 cluster and Pb_9Sb_9 cluster are more chemically stable based on the HOMO–LUMO gap analysis. The density of states of Pb_nSb_n (n = 2–12) clusters shift toward more negative energy levels with the growing cluster size n, and density of states becoming more nonlocalized with the increasing cluster size n.

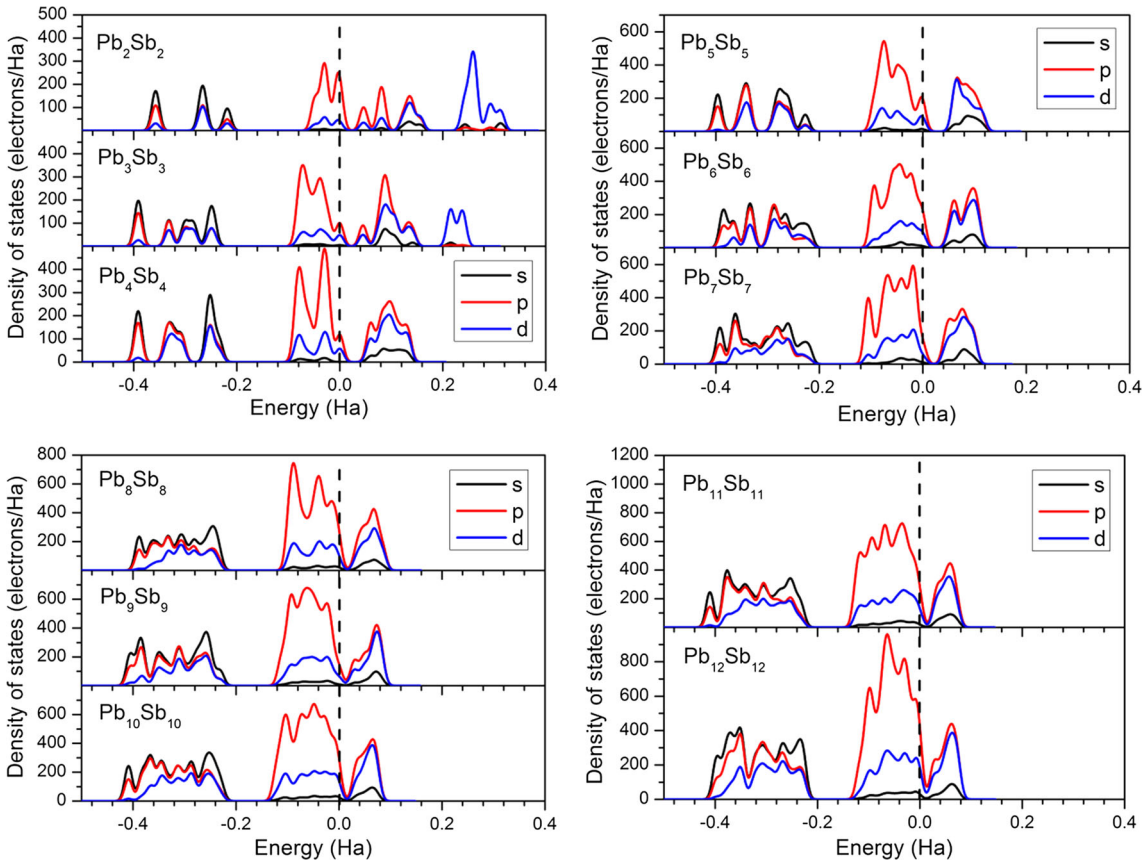

Fig. 5 Density of states of Pb_nSb_n (n = 2–12) clusters. The fermi level is viewed as a vertical dash line, and set to zero

Acknowledgements This work was supported by the Regional Foundation of the NSFC (51664032), General Program of the NSFC (51474116), Program of China Scholarships Council (No. 201808530022), Joint Foundation of the NSFC-Yunnan province (U1502271), Cultivating Plan Program for the Leader in Science and Technology of Yunnan Province (2014HA003), Program for Non-ferrous Metals Vacuum Metallurgy Innovation Team of Ministry of Science and Technology (2014RA4018), National Key Research and Development Program of China (2016YFC0400404), Youth Program of NSFC (51504115) and Program for Innovative Research Team in University of Ministry of Education of China (IRT_17R48), Science and Technology Talent Cultivation Plan of Yunnan Province, China (2017HB009).

References

1. M. L. Polak, G. Gerber, J. Ho, and W. C. Lineberger (1992). *J. Chem. Phys.* **97**, 8990–9000.
2. H. Yang, Y. Wang, X. Chen, X. Zhao, L. Gu, H. Huang, J. Yan, C. Xu, G. Li, J. Wu, A. J. Edwards, B. Dittrich, Z. Tang, D. Wang, L. Lehtovaara, H. Häkkinen, and N. Zheng (2016). *Nat. Commun.* **7**, 12809.
3. I. M. L. Billas, A. Châtelain, and W. A. de Heer (1994). *Science* **265**, 1682–1684.
4. O. A. Van and R. J. Saykally (1998). *Chem. Rev.* **98**, 2313–2357.
5. L. Belau, S. E. Wheeler, B. W. Ticknor, M. Ahmed, S. R. Leone, W. D. Allen, and M. A. Duncan (2007). *J. Am. Chem. Soc.* **129**, 10229–10243.
6. J. Hutter, H. P. Luethi, and F. Diederich (1994). *J. Am. Chem. Soc.* **116**, 750–756.
7. M. Haertelt, J. T. Lyon, P. Claes, H. J. De, P. Lievens, and A. Fielicke (2012). *J. Chem. Phys.* **136**, 114.
8. K. D. Rinnen and M. L. Mandich (1992). *Phys. Rev. Lett.* **69**, 1823–1826.
9. S. Heiles, S. Schäfer, and R. Schäfer (2011). *J. Chem. Phys.* **135**, 034303.
10. W. Qin, W. C. Lu, Q. J. Zang, L. Z. Zhao, G. J. Chen, C. Z. Wang, and K. M. Ho (2010). *J. Chem. Phys.* **132**, 214509.
11. S. Schäfer, B. Assadollahzadeh, M. Mehring, P. Schwerdtfeger, and R. Schäfer (2008). *J. Phys. Chem. A* **112**, 12312.
12. B. Assadollahzadeh, S. Schäfer, and P. Schwerdtfeger (2010). *J. Comput. Chem.* **31**, 929–937.
13. H. Li, Y. Ji, F. Wang, S. F. Li, Q. Sun, and Y. Jia (2011). *Phys. Rev. B* **83**, 075429.
14. X.-P. Li, W.-C. Lu, Q.-J. Zang, G.-J. Chen, C. Z. Wang, and K. M. Ho (2009). *J. Phys. Chem. A* **113**, 6217–6221.
15. R. K. Yoo, B. Ruscic, and J. Berkowitz (1992). *J. Chem. Phys.* **96**, 6696–6709.
16. X. Bai, Q. Zhang, A. Gao, and J. Yang (1009). *Comput. Theor. Chem.* **2013**, 94–102.
17. X. Zhou, J. Zhao, X. Chen, and W. Lu (2005). *Phys. Rev. A* **72**, 053203.
18. R. O. Jones, O. Ahlstedt, J. Akola, and M. Ropo (2017). *J. Chem. Phys.* **146**, 1291–12100.
19. T. M. Bernhardt, B. Kaiser, and K. Rademann (2002). *Phys. Chem. Chem. Phys.* **4**, 1192–1200.
20. X. Zhou, J. Zhao, X. Chen, and W. Lu (2005). *Phys. Rev. A* **72**, 053203.

21. J. J. Melko, U. Werner, R. Mitric, V. Bonacic-Koutecky, and A. W. Castleman Jr. (2011). *J. Phys. Chem. A.* **115**, 10276–10280.
22. D. Schild, R. Pflaum, G. Riefer, and E. Recknagel (1988). *Zeitschrift Für Physik D Atoms Molecules & Clusters* **10**, 329–335.
23. S. Yahachi, Y. Kenzi, M. Kazuhiro, and N. Tamotsu (1982). *Jpn. J. Appl. Phys.* **21**, L396.
24. C. Rajesh and C. Majumder (2007). *J. Chem. Phys.* **126**, 244704.
25. S. Schafer, S. Heiles, J. A. Becker, and R. Schafer (2008). *J. Chem. Phys.* **129**, 044304.
26. V. Senz, T. Fischer, P. Oelssner, J. Tiggesbaumker, J. Stanzel, C. Bostedt, H. Thomas, M. Schoffler, L. Foucar, M. Martins, J. Neville, M. Neeb, T. Moller, W. Wurth, E. Ruhl, R. Dorner, H. Schmidt-Bocking, W. Eberhardt, G. Gantefor, R. Treusch, P. Radcliffe, and K. H. Meiwes-Broer (2009). *Phys. Rev. Lett.* **102**, 138303.
27. C. Rajesh and C. Majumder (2008). *J. Chem. Phys.* **128**, 024308.
28. X. Chen, K. Deng, C. Xiao, J. Chen, and D. E. Ellis (2011). *Comput. Theor. Chem.* **971**, 73–76.
29. M. Steinert, W. Wesch, A. Undisz, M. Rettenmayr, W. Nunes, R. Borges, M. Godinho, R. Rubinger, M. Carmo, and N. Sobolev (2008). *J. Phys. D: Appl. Phys.* **42**, 035406.
30. R. W. Farley, P. Ziemann, and A. W. C. Jr (1989). *Zeitschrift Für Physik D Atoms Molecules & Clusters* **14**, 353–360.
31. R. Wheeler, K. LaiHing, W. Wilson, J. Allen, R. King, and M. Duncan (1986). *J. Am. Chem. Soc.* **108**, 8101–8102.
32. K. F. Willey, K. Laihing, T. G. Taylor, and M. A. Duncan (1993). *J. Phys. Chem.* **97**, (29), 7435–7440.
33. D. Schild, R. Pflaum, K. Sattler, and E. Recknagel (1987). *J. Phys. Chem.* **91**, 2649–2653.
34. J. J. Melko, S. V. Ong, U. Gupta, J. U. Reveles, J. D'Emidio, S. N. Khanna, and A. W. Castleman (2010). *Phys. Chem. C* **114**, 20907–20916.
35. E. C. Honea, A. Ogura, C. A. Murray, K. Raghavachari, W. O. Sprenger, M. F. Jarrold, and W. L. Brown (1993). *Nature* **366**, 42–44.
36. B. Wang, J. Zhao, X. Chen, D. Shi, and G. Wang (2005). *Phys. Rev. A* **71**, 309–315.
37. M. Bo, Y. Wang, Y. Huang, W. Zhou, C. Li, and C. Q. Sun (2014). *J. Mater. Chem. C* **2**, 6090.
38. B. Song, W. Jiang, B. Yang, X. Chen, B. Xu, L. Kong, D. Liu, and Y. Dai (2016). *Metall. Mater. Trans. A* **47**, 5214–5222.
39. J. Deng, Y. Lei, S. Wen, and Z. Chen (2015). *Int. J. Miner. Process.* **140**, 43–49.
40. G. L. Zhang, H. K. Yuan, H. Chen, A. L. Kuang, Y. Li, J. Z. Wang, and J. Chen (2014). *J. Chem. Phys.* **141**, 244304.
41. M. Zhang, L.-M. He, L.-X. Zhao, X.-J. Feng, and Y.-H. Luo (2009). *J. Phys. Chem. C* **113**, 6491–6496.
42. G. Gerber and G. Kuscher (1981). *Chem. Phys.* **60**, 119–131.
43. R. K. Yoo, B. Ruscic, and J. Berkowitz (1993). *J. Chem. Phys.* **99**, 8445–8450.
44. C. Rajesh, C. Majumder, M. G. R. Rajan, and S. K. Kulshreshtha (2005). *Phys. Rev. B* **72**, 235411.
45. M. E. Eberhart, R. C. O'Handley, and K. H. Johnson (1984). *Phys. Rev. B* **29**, 1097–1100.
46. X. Li, B. Kiran, L.-F. Cui, and L.-S. Wang (2005). *Phys Rev. Lett.* **95**, 253401.
47. Y.-R. Zhao, X.-Y. Kuang, B.-B. Zheng, Y.-F. Li, and S.-J. Wang (2011). *J. Phys. Chem. A* **115**, 569–576.
48. K. O. Alcantar-Medina, M. Herrera-Trejo, A. Tlahuice-Flores, S. Martinez-Vargas, J. Oliva, and A. I. Martinez (1099). *Comput. Theor. Chem.* **2017**, 55–63.
49. D. Toprek and V. Koteski (1081). *Comput. Theor. Chem.* **2016**, 9–17.
50. Y. Jin, G. Maroulis, X. Kuang, L. Ding, C. Lu, J. Wang, J. Lv, C. Zhang, and M. Ju (2015). *Phys. Chem. Chem. Phys.* **17**, 13590.
51. X. X. Xia, A. Hermann, X. Y. Kuang, Y. Y. Jin, C. Lu, and X. D. Xing (2016). *J. Phys. Chem. C* **120**, 677–684.
52. S. Safer, S. Mahtout, K. Rezouali, M. A. Belkhir, and F. Rabilloud (1090). *Comput. Theor. Chem.* **2016**, 23–33.
53. W. G. Sun, J. J. Wang, C. Lu, X. X. Xia, X. Y. Kuang, and A. Hermann (2017). *Inorg. Chem.* **56**, 1241–1248.